

Submicrometer photoresponse mapping of nanowire superconducting single-photon detectors

Robert H. Hadfield,^{a)} Paul A. Dalgarno, John A. O'Connor, Euan Ramsay, and Richard J. Warburton

School of Engineering and Physical Sciences, Heriot-Watt University, Edinburgh EH14 4AS, United Kingdom

Eric J. Gansen, Burm Baek, Martin J. Stevens, Richard P. Mirin, and Sae Woo Nam

National Institute of Standards and Technology, 325 Broadway, Boulder, Colorado 80305 USA

(Received 16 August 2007; accepted 21 November 2007; published online 13 December 2007)

We report on the photoresponse mapping of nanowire superconducting single-photon detectors using a focal spot significantly smaller than the device area ($10 \times 10 \mu\text{m}^2$). Using a confocal microscope configuration and solid immersion lens, we achieve a spot size of 320 nm full width at half maximum onto the device at 470 nm wavelength. We compare the response maps of two devices: The higher detection efficiency device gives a uniform response, whereas the lower detection efficiency device is limited by a single defect or constriction. © 2007 American Institute of Physics. [DOI: 10.1063/1.2824384]

Recent advances in optics and nanotechnology allow light-matter interactions to be probed on ever-diminishing length scales and hold the key to insights into fundamental physics and the development of new technologies. In this letter, we apply the techniques of nano-optics [namely, confocal microscopy¹ in conjunction with a high refractive index solid immersion lens (SIL)²⁻⁴] in order to focus light with submicrometer precision onto nanostructured superconducting wires and to map their photoresponse.

Superconducting single-photon detectors (SSPDs) based on superconducting nanowires hold promise as a new type of high-speed, high sensitivity single-photon detector, with a spectral range from the visible well into the infrared. The basic device concept was pioneered by Gol'tsman *et al.*⁵ A 100 nm wide wire is patterned by electron beam lithography and etching in an ultrathin (4 nm thick) NbN superconducting film. The superconducting wire (operated in the temperature range 1.5–4 K) is biased close to its critical current I_C : The arrival of a visible or infrared photon perturbs the current distribution, triggering a fast voltage pulse with picosecond rise time. The current generation of nanowire SSPD (Ref. 6) consists of a meander wire (100 nm linewidth, 200 nm period) covering a $10 \times 10 \mu\text{m}^2$ area, compatible with a single mode telecommunications fiber.⁷ These detectors have been successfully employed in a range of applications at the frontiers of science and technology, spanning quantum cryptography,^{8,9} quantum emitter characterization,¹⁰⁻¹⁴ time-of-flight ranging,¹⁵ testing of integrated circuits,¹⁶ and high-speed communications.¹⁷ Recent studies have highlighted the challenges in creating large area nanowire devices:^{18,19} Defects or constrictions arising from the basic film or during processing are believed to limit the device yield. To date, the presence of constrictions has been inferred indirectly from critical current^{18,19} and inductance¹⁹ measurements. Optical characterization can offer a direct measurement but has typically only been carried out using a focal spot significantly larger than the device area.^{6,20} In this study, we map the photoresponse of nanowire SSPDs with

unprecedented resolution. We study two devices and show that the higher detection efficiency (DE) device has a uniform photoresponse, whereas the lower DE device is photo-sensitive at just a single spot. Furthermore, this study serves to signpost new strategies for achieving efficient optical coupling to nanostructured detectors.

The mapping setup is shown in Fig. 1. This configuration allows excellent optical and spatial resolution, combining a confocal microscope (composed of aspheric lenses) with XYZ piezoelectric translation stages at 4.2 K. The camera assists optical alignment. The sample space is filled with He vapor and the microscope is immersed in liquid He. The resolution limit by Sparrow's criterion²¹ is

$$\text{FWHM} = \frac{0.52\lambda}{n\text{NA}}, \quad (1)$$

where FWHM is the full width at half maximum of the focal spot, λ is the wavelength, NA is the numerical aperture of the

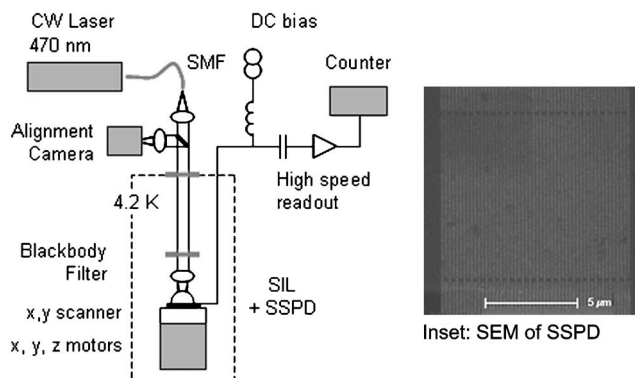


FIG. 1. Photoresponse mapping setup. This configuration affords high resolution scanning over a $12 \times 12 \mu\text{m}^2$ area without SIL and $6 \times 6 \mu\text{m}^2$ with $n=2.0$ SIL. The confocal microscope has a short working distance and high NA. The sample is mounted on a low temperature piezoelectric translation stage. The device is electrically connected for biasing and readout of photodetection events. SSPD, nanowire superconducting single photon detector; SIL, hemispherical solid immersion lens; SMF, single mode optical fiber; cw laser, continuous wave laser. Inset: a scanning electron micrograph (SEM) of a nanowire SSPD as used in this study (100 nm linewidth, 200 nm period, and $10 \times 10 \mu\text{m}^2$ area).

^{a)}Electronic mail: r.h.hadfield@hw.ac.uk.

objective lens, and n is the refractive index. This formula assumes plane wave illumination but gives a fair approximation for a truncated Gaussian beam. A high refractive index hemispherical SIL allows an enhancement in resolution (compared to free space) by a factor of n . This setup is routinely used in the spectroscopy of individual semiconductor quantum dots.^{3,22,23} We use a LaSFN35 glass SIL with $n=2.0$. XYZ piezomotors allow movement in sub-100-nm steps over a range of several millimeters, but with imperfect stitching characteristics. An additional XY piezoscanner stage allows precision scanning over a $12 \times 12 \mu\text{m}^2$ area. An indium tin oxide filter is placed in the optical path to reduce 300 K blackbody radiation. The minimum temperature attained by the sample stage is 4.9 K. Photodetection events are read out from the SSPD via a bias tee and high-speed room temperature amplifiers, feeding pulses into a counter.

For this study, we selected two nanowire SSPDs of equal dimensions (100 nm linewidth, 200 nm period, and $10 \times 10 \mu\text{m}^2$ area), but differing DE and electrical properties. A scanning electron micrograph (SEM) of one of these devices is shown in Fig. 1, inset. Using our standard fiber coupling technique in a closed-cycle adiabatic demagnetization refrigerator, the first device had a DE of 0.3% at $\lambda=550$ nm at 4.0 K and 0.5% at 1 K and an ungated dark count rate of 1 kHz. The inductance of this device measured at 4.0 K showed an upturn of 8% toward I_C of $22 \mu\text{A}$ [Fig. 2(a), inset (ii)], indicating that a large proportion of the wire is biased close to the critical current density (J_C).¹⁹ The absolute inductance value is strongly dependent on film thickness and composition and gives little indication of device quality. In contrast, the DE of the second device when fiber coupled was 10^{-6} at $\lambda=1550$ nm (1 kHz dark count) and 4.0 K. I_C at 4.0 K was just $3 \mu\text{A}$. The inductance of this device changes by less than 2% toward the I_C [Fig. 2(b), inset (ii)], indicating that most of the wire is biased well below J_C , owing to a defect or constriction in the nanowire.¹⁹

We mounted the higher DE SSPD in the confocal microscope (Fig. 1). Using an objective with a NA of 0.4 (but no SIL), we mapped the entire device using a continuous wave (cw) laser at $\lambda=470$ nm and a pulsed diode laser at $\lambda=410$ nm at 4.9 K. A qualitatively identical response was seen in both cases over a range of bias points and photon fluxes. Figure 2(a) shows a uniform plateau over the full $10 \times 10 \mu\text{m}^2$ device area, with counts per second acquired at each point. The background count rate for this scan was ~ 100 Hz. The photon flux was 10^8 photons/s. The photoresponse varies across the device by just a factor of 2, with broad peaks in two regions of the device separated by a slight diagonal trough. The spot resolution is determined from fitting the profile at the device edge. The differentiated fit yields a spot profile (640 nm FWHM) close to the resolution expected from Eq. (1) (610 nm FWHM). DE for the focused spot positioned on the most sensitive area of the device was 0.2% at 1 kHz ungated dark count rate. This is a fair correspondence to the fiber-coupled measurements on this device, although one would expect improved DE due to the shorter wavelength¹⁰ and the improved optical coupling. In these scanning measurements, the thermal environment and blackbody load on the device differ from the fiber-coupled experiments, resulting in an elevated operating temperature (4.9 K) and a reduction in DE at a given dark count rate.

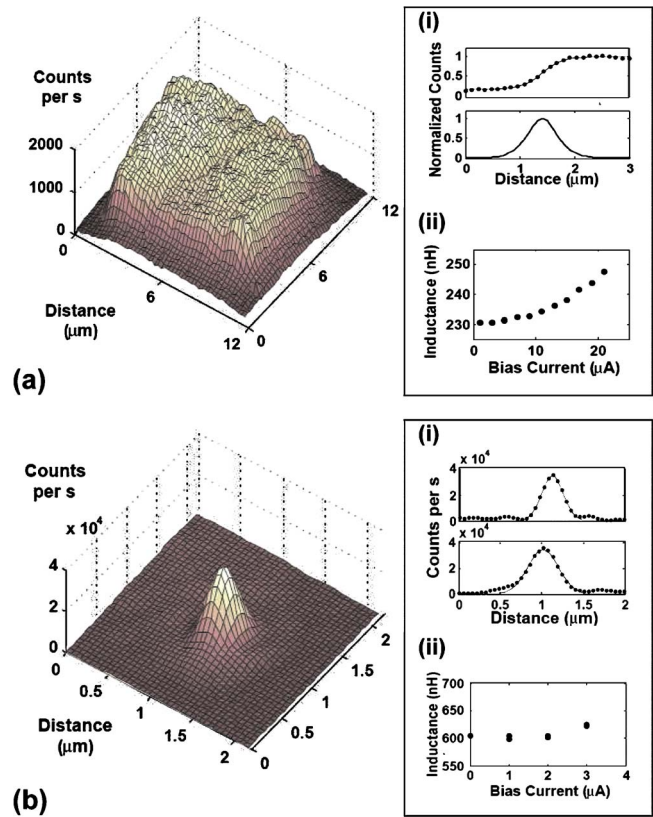


FIG. 2. (Color online) Photoresponse signatures of nanowire SSPDs (using setup depicted in Fig. 1). Sample temperature of 4.9 K. (a) Higher detection efficiency (DE) $10 \times 10 \mu\text{m}^2$ area device. No SIL, $\text{NA}=0.4$, $\lambda=470$ nm, and scanning area $12 \times 12 \mu\text{m}^2$. Inset (i): upper trace, profile of high resolution scan over edge with fit. In the lower trace, the FWHM from the differentiated fit is 620 nm. Inset (ii): inductance versus bias current at 4.0 K. The inductance at zero bias is 230 nH and increases by 8% toward the critical current ($22 \mu\text{A}$). (b) Lower DE $10 \times 10 \mu\text{m}^2$ area device. SIL $n=2.0$, $\text{NA}=0.36$, $\lambda=470$ nm, and high resolution scan of $2.16 \times 2.16 \mu\text{m}^2$ area. Inset (i): profiles in orthogonal scanning directions. FWHM from Gaussian fits: 313 and 430 nm, respectively. Inset (ii): inductance versus bias current at 4.0 K. The inductance at zero bias is 600 nH and increases by 3% toward the critical current ($3 \mu\text{A}$).

We then mapped the lower DE SSPD at $\lambda=470$ nm in the same setup. We employed a hemispherical SIL ($n=2.0$) and lens with $\text{NA}=0.36$ to enhance the optical resolution (the increased magnification reduces the overall scan range by a factor of n , to $6 \times 6 \mu\text{m}^2$). The full device area was mapped in a sequence of scans. The device responds at just a single point. Figure 2(b) shows a photoresponse map centered on the single photosensitive spot over a $2.16 \times 2.16 \mu\text{m}^2$ area. A qualitatively identical response was seen over a range of bias points and photon fluxes. The FWHMs of the peak (from a Gaussian fit) in orthogonal directions are 313 and 440 nm [inset (ii)], which are close to the theoretical resolution limit [Eq. (1) yields a FWHM of 340 nm]. The Airy disk profile is exaggerated by spherical aberrations and the SIL; the slight asymmetry in the lower profile can be attributed to tilt in the optical path. We can therefore confirm that the sensitive spot is significantly smaller than the optical resolution. Using these enhanced optics, the maximum DE was 10^{-5} (at 1 kHz dark count rate), again indicating that the sensitive area is much smaller than our spot size.

In conclusion, we have mapped the photoresponse of nanowire SSPDs with a focal spot significantly smaller than the device area. We have mapped two SSPDs of contrasting

performance: The higher DE device gives a uniform response across the device area, whereas the lower DE device responds at a single point where the nanowire is constricted. We intend to implement a similar scanning setup to image these devices at longer wavelengths (beyond 1 μm). A hyperhemispherical Si super SIL ($n=3.5$) with an NA=0.4 lens would confer a spot size at $\lambda=1550$ nm of 160 nm (Ref. 24) and ~ 110 nm at $\lambda=1064$ nm, allowing us to probe the photoresponse signature of single wires. Photoresponse mapping experiments on conventional Si APD single-photon detectors have yielded significant insights into the spatial dependence of device sensitivity and timing response;²⁵ we are now in a position to undertake similar studies on nanowire SSPDs, over much finer length scales. Furthermore, this enhanced optical coupling technology will allow us to explore novel device designs (e.g., nanoantennas), which may prove easier than the current meander design to fabricate with high yield and to scale up into multipixel arrays.

This work was supported by the Royal Society of London and EPSRC (United Kingdom) and DARPA, DTO, and the NIST Quantum Information Science Initiative (USA). The authors thank Gregory Gol'tsman for providing the original devices used in this study and thank Aaron Miller and Alan Migdall for useful discussions.

¹R. H. Webb, Rep. Prog. Phys. **59**, 427 (1996).

²S. M. Mansfield and G. S. Kino, Appl. Phys. Lett. **57**, 2615 (1990).

³V. Zwiller and G. Bjork, J. Appl. Phys. **92**, 660 (2002).

⁴W. L. Barnes, G. Bjork, J. M. Gerard, P. Jonsson, J. A. E. Wasey, P. T. Worthing, and V. Zwiller, Eur. Phys. J. D **18**, 197 (2002).

⁵G. N. Gol'tsman, O. Okunev, G. Chulkova, A. Lipatov, A. Semenov, K. Smirnov, B. Voronov, A. Dzardanov, C. Williams, and R. Sobolewski, Appl. Phys. Lett. **79**, 705 (2001).

⁶A. Verevkin, J. Zhang, R. Sobolewski, A. Lipatov, O. Okunev, G. Chulkova, A. Korneev, K. Smirnov, G. N. Gol'tsman, and A. Semenov, Appl. Phys. Lett. **80**, 4687 (2002).

⁷SMF-28e optical fiber, www.corning.com.

⁸R. H. Hadfield, J. L. Habif, J. Schlafer, R. E. Schwall, and S. Nam, Appl. Phys. Lett. **89**, 241129 (2006).

⁹H. Takesue, S. Nam, Q. Zhang, R. H. Hadfield, T. Honjo, K. Tamaki, and Y. Yamamoto, Nat. Photonics **1**, 343 (2007).

¹⁰R. H. Hadfield, M. J. Stevens, S. S. Gruber, A. J. Miller, R. E. Schwall, R. P. Mirin, and S. W. Nam, Opt. Express **13**, 10846 (2005).

¹¹M. J. Stevens, R. H. Hadfield, R. E. Schwall, S. W. Nam, R. P. Mirin, and J. A. Gupta, Appl. Phys. Lett. **89**, 031109 (2006).

¹²C. Liang, K. F. Lee, M. Medic, P. Kumar, R. H. Hadfield, and P. Kumar, Opt. Express **15**, 1322 (2007).

¹³R. H. Hadfield, M. J. Steven, S. Nam, and R. P. Mirin, J. Appl. Phys. **101**, 103104 (2007).

¹⁴C. Zinoni, B. Alloing, L. H. Li, F. Marsili, A. Fiore, L. Lungi, A. Gerardino, Yu. B. Vakhtomin, K. V. Smirnov, and G. N. Gol'tsman, Appl. Phys. Lett. **91**, 031106 (2007).

¹⁵R. E. Warburton, A. McCarthy, A. Walker, S. Hernandez-Marin, R. H. Hadfield, S. Nam, and G. S. Buller, Opt. Lett. **32**, 2266 (2007).

¹⁶J. Zhang, N. Boiadjeva, G. Chulkova, H. Deslandes, G. N. Gol'tsman, A. Korneev, P. Kouminov, A. Leibowitz, W. Lo, R. Malinsky, O. Okunev, A. Pearlman, W. Slyz, K. Smirnov, C. Tsao, A. Verevkin, B. Voronov, K. Wilsher, and R. Sobolewski, Electron. Lett. **39**, 1086 (2003).

¹⁷B. S. Robinson, A. J. Kerman, E. A. Dauler, R. O. Barron, D. O. Caplan, M. L. Stevens, J. J. Carney, S. A. Hamilton, J. K. W. Yang, and K. K. Berggren, Opt. Lett. **31**, 444 (2006).

¹⁸F. Mattioli, R. Leoni, A. Gaggero, M. G. Castellano, P. Carelli, F. Marsili, and A. Fiore, J. Appl. Phys. **101**, 054302 (2007).

¹⁹A. J. Kerman, E. A. Dauler, J. K. W. Yang, K. M. Rosfjord, V. Anant, K. K. Berggren, G. N. Gol'tsman, and B. M. Voronov, Appl. Phys. Lett. **90**, 101110 (2007).

²⁰K. M. Rosfjord, J. K. W. Yang, E. A. Dauler, A. J. Kerman, V. Anant, B. M. Voronov, G. N. Gol'tsman, and K. K. Berggren, Opt. Express **14**, 527 (2006).

²¹C. M. Sparrow, Astrophys. J. **44**, 76 (1916).

²²S. Moehl, H. Zhao, B. D. Don, S. Wachter, and H. Kalt, J. Appl. Phys. **93**, 6265 (2003).

²³P. A. Dalgarno, J. McFarlane, B. B. Geradot, R. J. Warburton, K. Karrai, A. Badolato, and P. M. Petroff, Appl. Phys. Lett. **89**, 043107 (2006).

²⁴E. Ramsay, K. A. Serrels, M. J. Thomson, A. J. Waddie, M. R. Taghizadeh, R. J. Warburton, and D. T. Reid, Appl. Phys. Lett. **90**, 131101 (2007).

²⁵M. Ware, A. Migdall, J. C. Bienfang, S. V. Polyakov, and J. Modern, J. Mod. Opt. **54**, 361 (2007).